Design-based Stereology to Quantify Structural Properties of Artificial and Natural Snow Using Thin Sections

F. Riche [a], M. Schneebeli [a], S.A. Tschanz [b]

[a] WSL Institute for Snow and Avalanche Research SLF, [b] Institute of Anatomy, University of Bern

Corresponding author:

F. Riche

WSL Institute for Snow and Avalanche Research SLF, Flüelastrasse 11,7260 Davos Dorf

riche@slf.ch

Phone: +41 81 417 01 11

This document is the accepted manuscript version of the following article:
Riche, F., Schneebeli, M., & Tschanz, S. A. (2012). Design-based stereology to quantify structural properties of artificial and natural snow using thin sections. Cold Regions Science and Technology, 79-80, 67-74. https://doi.org/10.1016/j.coldregions.2012.03.008

ABSTRACT

The quantification of the structural properties of snow is traditionally based on model-based stereology. Model-based stereology requires assumptions about the shape of the investigated structure. Here, we show how the density, specific surface area, and grain boundary area can be measured using a design-based method, where no assumptions about structural properties are necessary. The stereological results were also compared to X-ray tomography to control the accuracy of the method. The specific surface area calculated with the stereological method was 19.8 ± 12.3% smaller than with X-ray tomography. For the density, the stereological method gave results that were 11.7 ± 12.1% larger than X-ray tomography. The statistical analysis of the estimates confirmed that the stereological method and the sampling used are accurate. This stereological method was successfully tested on artificially produced ice beads but also on several snow types. Combining stereology and polarisation microscopy provides a good estimate of grain boundary areas in ice beads and in natural snow, with some limitations.

KEYWORDS: Snow, design-based stereology, specific surface area, grain boundary, x-ray tomography

1. Introduction

Stereology is an analytical and statistical method used to quantify three-dimensional properties from plane (two-dimensional) sections, without the need to reconstruct the three-dimensional structure (Howard and Reed, 1998). Stereology is often used in materials science and biology and can provide quantitative information regarding the geometrical properties of the sample, such as volume, surface

area, and length (Baddeley et al., 1986; Gundersen and Jensen, 1985; Howard and Reed, 1998). Other properties such as the number of structural components or the mean particle size can also be obtained with more sophisticated sampling approaches (Cruz-Orive and Weibel, 1981; Fisher et al., 1988; Sterio, 1984). Sampling procedure and counting strategy are the two important steps used to obtain accurate results and to avoid any methodical or systematic bias (Gundersen et al., 1999; Tschanz et al., 2011). Two principal stereological approaches exist: model-based stereology and design-based stereology (Baddeley et al, 1986) (details in section "2. Theory"). Here, a design-based method is presented, which can be used specifically for snow and porous ice samples. The evaluation of digitally captured images is done by free software (e.g., ImageJ, STEPanizer), but commercial packages (e.g., newCAST, Visiopharm, Hoersholm, Danmark) can also be used.

As early as 1936, techniques used to produce thin sections of snow were described (Bader et al., 1939). The key point for preparing snow in thin sections is to fill the pore space with a super-cooled liquid (such as diethyl-phthalate), which is frozen to obtain a rigid and solid sample. Then, the sample can be cut with a microtome to obtain a surface plane, which can be observed through a microscope. Buser and Good (1987) and (Davis and Dozier, 1989) used superimposed linear grids to analyse, through stereology, some snow properties. They measured the surface area and mean linear intercept-length to evaluate the pore space and the average number of grains per unit volume. The specific surface area (SSA) is an important property of the snow microstructure. For this reason, several studies use stereological methods to quantify the SSA (Arakawa et al., 2009; Arnaud et al., 2011; Matzl and Schneebeli, 2010). However, all of these methods assume some geometrical isotropy in the snow and would probably exhibit measurement bias in a very anisotropic structure such as a depth hoar.

With thick sections (also called surface sections), it is sometimes possible to observe grain boundaries. This is based on the sublimation of ice, but the method is difficult and not efficient because it is hard to find the precise conditions to have optimal sublimation of ice at the grain boundaries (Arnaud et al., 1998). The method works well for firm and dense snow but becomes increasingly difficult with higher

porosity.

The surface area (SA) and grain boundaries (GB) of ice crystals are important for snow chemistry because trace gases and impurities are located there (Domine et al., 2008). GB could also contain a reservoir of trace gases (Huthwelker et al., 2006). In this context, a grain is defined as a structural unit belonging to the same ice crystal orientation. Therefore, the grain boundary area (GBA) is an important structure for chemical properties of snow and the mechanical deformation of the snow structure. Temporal and spatial changes in GBAs have never been measured before.

X-ray tomography cannot detect grain boundaries. In some particular cases, when GBA corresponds to a particular geometry of the structure, the GBAs can be calculated with the help of image processing (Theile and Schneebeli, 2011). For this reason, the preparation of thin sections observed under polarised light and the use of stereology are necessary to quantify GBA bias-free, irrespective of their location.

In an isotropic material, the light propagates at the same velocity in every direction. Ice is a birefringent crystal and is optically anisotropic. Hence, white light passes through crossed polarisers, causing crystals with a different orientation of the optical axes to appear in different colours (Hobbs, 2010). To summarise, with the use of a crossed polariser, the orientation of the crystal axis produces coloured grains. The GB can then be identified precisely as the line between two different colours. To observe and quantify the GBs in snow, thin sections of the snow (100 µm - 150 µm) were made.

A stereological method was developed to quantify, without bias, the GBs and the polycrystalline properties of ice as well their geometry (SSA, volume density). Micro-computed tomography (µCT) was used to check the validity and accuracy of our stereological method. This method was developed initially for artificial ice beads (Riche and Schneebeli, 2011) because they are widely used in “snow” chemistry experiments. However, natural snow can also be quantified with this stereological method. We performed some tests on natural snow in the form of rounded grains and depth hoar.

2 Theory

Stereology is a collection of methodological concepts that permit the extraction of information from plane sections of three-dimensional materials. It is based on statistical principles and gives an estimate of the properties of interest. The concepts are simple and efficient because, most of the time, they only use raw images (without any image processing) from optical microscopy and a minimum of plane sections of the material to be analysed (Baddeley and Vedel Jensen, 2005; Howard and Reed, 1998). Basically, a stereologic study consists of two major steps: (a) unbiased material sampling and (b) quantification of structures by feature counts.

Formerly, thin or thick sections were quantified directly under the microscope using a projection screen or a transparency superposing the suitable test system (e.g., cycloids). Currently, some software exists to simplify the counting procedure. An example is the STEPanizer, which is free.

In stereology, two principal approaches exist: (1) model-based stereology is based on assumptions of the geometric properties of the sample, and (2) design-based stereology (Baddeley et al, 1986), where no assumptions are made on the geometry. Here, we detail these two approaches.

1) Model-based stereology

Model-based stereology is the more traditional approach of stereology. The material is assumed to be spatially homogeneous. Therefore, the 3D structural properties of the material can be extracted from only one arbitrary plane section of this material. Model-based stereology is prone to bias and should progressively be replaced by assumption-free approaches.

In snow, the model-based method (Davis and Dozier, 1989) assumed a sphere-like geometry and an isotropic structure. The model-based method of Matzl and Schneebeli (2010) assumed rotational isotropy in the vertical direction.

113

114 **2) Design-based stereology**

115 This approach is mathematically designed in such a way that quantification is independent of the
116 structural size and dimension as well as its distribution and spatial orientation (Gundersen, 1988; West,
117 1993). Design-based approaches are bias-free with respect to all structural properties, if sampling is
118 already unbiased and accurate (Baddeley et al., 1986; Howard and Reed, 1998).
119 To realise unbiased sampling, sections have to be produced according to specific random sampling
120 procedures (also called random sampling design).
121 Here, we present a design-based approach that can be used specifically in snow and porous ice samples.
122 It includes the section sampling procedure, taking any structural anisotropy into account, as well as the
123 quantification of grain boundaries.

124

125 # 3 Methods

126

127 ## 3.1 Sample production

128

129 Ice beads were prepared from water droplets. The droplets were frozen in liquid nitrogen and formed
130 ice beads of different sizes. The ice beads were then sieved to a fraction between 600 µm and 500 µm,
131 which was kept for the experiments.
132 Sample holders (20 mm in diameter and 5 cm high) used for µCT measurements and small boxes (3 cm
133 in diameter and 1 cm high) for thin section preparation were then filled with the ice beads. Samples
134 were carefully stored in an isothermal box to keep a constant temperature in and around the samples in
135 case of small temperature variations in the freezers (Lowe et al., 2011). As all of the samples were
136 prepared and stored in an isothermal box together, we assumed that all of the ice bead samples had the

same structural evolution and could therefore be compared (stereology measurements versus µCT measurements).

Sample holders were scanned with the µCT, and boxes were taken to prepare thin sections for polarisation microscopy. Eighteen samples were analysed. Furthermore, three samples of natural snow of different snow types (small rounded grains and 2 depth hoar samples) were also analysed.

3.2 Stereological section sampling

Unbiased sampling is the crucial step in a stereological approach to receive an accurate quantitative estimation. Every part of the sample must have the same probability of belonging to the sample used for the measurement. One section sampling approach used in design-based stereology, to avoid bias from structural anisotropy, is called vertical uniform random sections (VUR). VUR sections have to be prepared following these three main steps: (1) Selecting a horizontal reference plane (the vertical axis is therefore perpendicular to the reference plane), (2) randomly rotating the material around the vertical axis, and (3) cutting sections parallel to the vertical axis (Howard and Reed, 1998).

In our approach, the VUR section method was chosen, and three random vertical sections per sample were cut. The three sections were cut with systematic randomness with regards to orientation and position as shown in Figure 2. This procedure required nine steps.

For stereological quantification based on the vertical section design, it is crucial to know the vertical axis on each section. The top and bottom of the snow pellet should correspond to the upper or bottom border of the section. This is true if the cut (cuts A - C) is perpendicular to the top and bottom of the pellet.

3.3 Thin section preparation

Thin sections were produced following the experimental procedures described in the literature (Good, 1987; Kinosita and Wakahama, 1959; Satyawali et al., 2003) but with slight modifications. The procedure used is described here in detail.

The small boxes were slowly filled with di-ethyl phthalate (CAS 84-66-2) at -4°C (in comparison to di-methyl phthalate, di-ethyl phthalate is less toxic). Once frozen, the sample was cut without destroying the ice bead structure. Thin sections were prepared using a microtome (Leica Polycut) with a thickness of 120 µm to 150 µm. After the completion of the vertical section sampling design, the small pieces of the sample were glued with a drop of di-ethyl phthalate on a glass plate. To have a homogeneous thickness, a ring of ice was prepared and levelled with the knife of the microtome. The sample was placed on this ice ring, which was exactly parallel to the knife. The thickness of the sample therefore had an equal thickness everywhere. A vacuum pump sucked the air out of the ice ring in order to fix the sample onto the ring during cutting. Once the sample was completely flat, it had to be released from the glass plate and glued again to the other side. To glue the sample on its second side, it was warmed to -2°C on a temperature controlled heater. Immediately after, the other side was fixed on a second glass plate. The second side then lay almost perfectly parallel to the knife, and a surface of equal thickness was cut. After covering the surface with a class cover, a drop of tetralin (CAS 119-64-2) was applied on the edge of the thin section to dissolve the diethyl-phthalate. Afterwards, the thin section could be observed with a polarisation microscope.

3.4 Stereological estimation

First, the different types of grain boundaries were defined (Fig. 3):

- **Surface area** (SA): ice-air interfaces, interfaces between ice crystals and air.
- **Grain boundary** (GB): ice-ice interfaces, interfaces between two ice crystals with a different

187 orientation, which is further subdivided into the following:

188 **- Internal grain boundary area** (IGBA): GB inside one ice bead,

189 **- Grain boundary area** (GBA): area between two geometrical ice beads.

190

191 Once the sections were prepared for polarisation microscopy, the different structures of interest of the
192 ice bead samples and the snow samples were analysed. Approximately 60 images (20 per section) were
193 evaluated to quantify the specific surface area (SSA), the specific grain boundary area (SGBA), and the
194 specific internal grain boundary area (SIGBA). The density of the sample and the percentage of
195 polycrystalline grains were also evaluated. The volume density was assessed by counting points of a
196 test system, hitting the structures of interest. Surface density was assessed by counting line (cycloid)
197 intersections with the GBs visible on the microscopic images. In a vertical section design, lines must
198 have a cycloid form (Baddeley et al., 1986). The STEPanizer software was used for counting (version
199 1, 0.22, http://www.stepanizer.com/; Tschanz et al., 2011). STEPanizer allows quantification of
200 microscopic images. Test systems (for example, a cycloid grid) are easily created and superimposed
201 onto the digital images. In the approach used, the ends of the cycloids (see Fig. 4) were used as
202 sampling points for the volume density estimation. The STEPanizer also facilitates the counting
203 process and transfers the data to a text file for further calculations. The number of cycloids has to be
204 adjusted according to the size of the structure. Before measuring, the optimal length and number of
205 cycloids must be empirically determined. Too many cycloids would result in a long counting procedure
206 and would not give better results than with less. Too few cycloids would not produce enough counts per
207 sample and would thus result in a poor estimate. For stereological evaluations, approx. 200 to 300
208 counts per sample are ideal (Gundersen and Osterby, 1981; Mathieu et al., 1981).

209

210 The structural properties were calculated by the following formulas:

211

Surface area density [mm^{-1}]:

$$S_v = \frac{2I}{(l/p)P_{ref}} \quad (1),$$

where *l/p* is the length of the test line per point, and P_{ref} is the number of points hitting the reference space. The reference space corresponds to the full area within a counting frame if captured images fully cover this frame. *I* is the number of intersections between the test lines (cycloids, red lines) and the structure of interest: SA, GBA or IGBA. It gives the surface area density per unit volume: SA_v, GBA_v and $IGBA_v$, respectively. The surface area density is the area per volume, and in this case, the units are mm^2/mm^3, which cancel to mm^{-1}.

Volume density of ice:

$$\rho_v = \frac{P_{ice}}{P_{ref}} \quad (2),$$

where P_{ice} are the number of points hitting the ice structure, and P_{ref} are the number of points of the reference space. Putting formulas (1) and (2) together allows the computation of

Specific areas per ice volume [mm^{-1}]:

$$S_{ice} = \frac{S_v}{\rho_v} = \frac{2I}{(l/p)P_{ice}} \quad (3),$$

Equation (3) permits the calculation of the different specific surfaces relative to ice, i.e., specific surface area (SSA), specific grain boundary area (SGBA) and specific internal grain boundary area (SIGBA).

Percentage of polycrystalline ice beads [%]:

$$\%Beads_{poly} = \frac{P_{beads\ poly}}{P_{ice}} 100, \quad (4),$$

where $P_{beads\ poly}$ is the number of points hitting polycrystalline ice beads, and P_{ice} is the number of points hitting the ice beads.

For all of these evaluations, we only considered the structure belonging to the surface of the 2D section, meaning that the black area surrounding the ice beads was discarded. The black area appeared because of the thickness of the section; therefore, it does not belong to the surface used for counting (Fig. 4).

Coefficient of error of a ratio estimate ($_{est}$CE) and coefficient of variation (CV):

The coefficient of error (CE) provides information about the variance of an estimate depending on the stereological procedure. The coefficient of variation (CV) expresses the total variance of a population (in our case, the snow samples). If the CE is much smaller than the CV the stereological estimate has a high accuracy. Accuracy means that the measurement is unbiased. In other terms, the measurement converges to a stable value and has a small standard deviation. Therefore, differences between populations will be detected (Howard and Reed, 1998). In contrast to image processing techniques, the estimate calculated from the stereological method is based on a rigorous statistical framework.

To calculate the CE and CV, the following formulas are used (Howard and Reed, 1998):

$$_{est}CE(\hat{R}_v) \approx \left[\frac{k}{k-1} \left\{ \frac{\sum u^2}{\sum u \sum u} + \frac{\sum v^2}{\sum v \sum v} - 2\frac{\sum uv}{\sum u \sum v} \right\} \right]^{(1/2)} \quad (5),$$

where k is the number of pictures, u is the number of points hitting the reference space and v is the number of intersection points (intersections between the test lines (cycloids, red lines) and the structure

of interest (SA, GB or IGB)).

$$CV(R) = \frac{\sigma}{\mu} \quad (6),$$

with $\mu = \frac{1}{N}\sum_{i=1}^{N} R_i$ (7) and $\sigma^2 = Var(R) = \frac{1}{N}\sum_{i=1}^{N}(R_i - \mu)^2$ (8),

with the variance σ and the mean μ, and where N is the number of pictures and R_i is the number of intersection points.

3.5 X-ray tomography

Samples were scanned in a 20-mm diameter sample holder, which was also the storage holder (no transfer of the ice beads was necessary). The scanned height of the sample was 4.16 mm. The original 3D image resolution was 10 µm.

The image processing language, IPL (Scanco Medical), was used for the segmentation of the 3D images. A block of 400 x 400 x 400 voxels (i.e., a block of 4 mm^3) was cut out at a fixed position. A Gauss filter was used on this volume (sigma = 1, support = 2), and then an adaptive threshold was applied to segment the measured structure in a binary volume with air and ice structures (Fig. 1). The adaptive threshold searches for the minimum between the peaks of the histogram of the grey-scale 3D image. The SSA, volume density, grain thickness and pore size of the segmented volumes were evaluated with IPL (image processing language) (Hildebrand and Ruegsegger, 1997; Kaempfer et al., 2005). The representative elementary volume (REV) is the minimal reasonable volume, which is necessary to define a macroscopic property of a material (Brown et al., 2000). The REV was large enough for this analysis, according to (Kaempfer et al., 2005), which suggests a size of larger than three to four structural elements in each dimension for the density estimation. For the ice beads, it would correspond to ~2 mm^3. The resolution was also 3 times higher than that proposed by (Flin et al.,

2011), and the analysed volume of 4 mm^3 was 1.6 times bigger than the minimum REV proposed in (Flin et al., 2011).

4. Results

4.1 Thin sections and polarisation microscopy

Using thin section and polarisation microscopy, the different crystals could be differentiated. The geometrical bond as well as the internal grain boundary were recognised. We observed polycrystalline and monocrystalline beads (Fig. 5).

4.2 Stereology

4.2.1 SSA and density, comparison to µCT

The SSA for the ice beads was between 6-9 mm^{-1}. This was slightly smaller than the values of the µCT evaluations. Considering all samples, the SSA measured by stereology was 1% to 28% smaller than that measured with the µCT (Fig. 6, Table 1), with an average of -19.8% and a standard deviation of 12.3%.

Density was slightly higher with the stereological method than with the µCT evaluation. A volume density of ~ 65% with the stereological method and ~ 60% with the µCT was obtained. When all samples were considered, the µCT produced a density that was 1% to 23% lower than the stereological method (average of 11.7%, standard deviation 12.1%) (Fig. 6, Table 1).

The CE from stereology is always much smaller than the CV (CE =~0.02 and CV = [0.04-1.64]). This

means that the stereological estimates have a high accuracy.

4.2.2 Quantification of grain boundaries and polycrystalline ice beads

The SGBA was between 1 - 2 mm^{-1}, and the SIGBA was between 4 - 6 mm^{-1} (Table 1).
The percentage of polycrystalline ice beads was between 60% and 70% of the total ice volume. The SGBA for ice bead samples and the rounded-grain snow were also compared to the values given by image processing based on the method of (Theile and Schneebeli,2011) (Fig. 8). The image processing method provides a minimum value and a maximum value of the SGBA, depending on the chosen filter parameters. The stereological estimates of the SGBA were almost always between these intervals, and when not, the value of the stereology estimate was very close to either the minimum or maximum (Table 2). At least for rounded-grain snow, it was possible to estimate the size and distribution of bonds without thin sections. However, internal grain boundaries could not be detected. The ratio of SGBA over SSA was 17.5 ± 3.2 % for the ice beads, which is similar to the ratio found by (Flin et al., 2011) with a computer simulation based on a grain segmentation algorithm.

4.3 Application to natural snow

The stereological method was also tested on natural snow samples. Here, snow with small rounded grains (Fig. 9a) and depth hoar (Fig. 9b) are shown. To cut thin sections for snow, the same technique as for ice beads was used. Table 3 summarises these results. The relative error between stereology and X-ray tomography is similar compared to the ice bead measurements. We also prepared a sample with new snow. However, in this case, the grain boundaries were very small and few, such that a quantitative evaluation was not possible.
The SGBA was compared to the image-processing algorithm for the small rounded grains (Table 2). In

the case of depth hoar, the geometry of the snow is too complex to find the correct GBAs with the computer simulation (Theile and Schneebeli, 2011). Comparison with the data of (Flin et al., 2011) shows a similar SGBA/SSA ratio for small rounded grains. For depth hoar, we found ratios (SGBA/SSA) of 24.6% and 22.1%, which are much lower that the ratio of (Flin et al., 2011) for similar snow types (ratio of ~ 40% for depth hoar). However, the snow samples were not the same and could not be directly compared.

5. Discussion

The ice beads have a much larger total GBA than would be estimated by their geometry because some grains are polycrystalline. For example, with the image processing technique using X-ray tomography measurements (Theile and Schneebeli, 2011), only the GBA that can be structurally recognised are found (Fig. 8); therefore, using only X-ray tomography with image processing would result in an underestimation of the GBA for the ice beads samples.

The differences between the stereology measurements and the μCT measurements can be explained by the following sources of error. First, for the μCT measurements, this difference could have been caused by a slightly high threshold in the image segmentation. However, the segmentation algorithms did not show systematic biases compared to gas adsorption (Kerbrat et al., 2008). One of the pit-falls of automated image processing approaches based on threshold segmentation is the difficulty in determining the appropriate threshold level. Its modification would result in unforeseeable and confusing area and volume density changes. A second explanation, which originates from the stereological measurement, is the following: even thin sections of ice beads or snow have a noticeable thickness (Fig. 7). Visually, the thickness of the sample appears either dark or out of focus on the images. Both surfaces do not count for the stereological measurements but are sometimes difficult to

351 discriminate from the “true” surface. Therefore, it is possible that, inadvertently, too much ice structure
352 is taken into account during the counting process, leading to an overestimation of the volume density.
353 Because the SSA is inversely proportional to the volume density, an overestimation of the volume
354 density will result in an underestimation of the SSA. This effect can be observed with the relative errors
355 listed in Table 1. When the SSA relative error is negative, the density relative error is positive (Fig. 6).
356 It also seems that these errors are, for most of the measurements with the ice beads, correlated.
357 However, a given correlation function, permitting to correct the SSA and density data could only be
358 valid for the ice beads because they always have approximately the same SSA over density ratio due to
359 their similar structures.
360 In addition, the stereological method and the µCT volume estimation are dealing with physically
361 different samples; therefore, some sample variability must be expected.
362 The CE is always much small than the CV, which confirms a high accuracy of the stereology estimates.
363 However, a systematic bias, which is caused by the observer, cannot be excluded and seems to be the
364 most difficult part in using stereology for snow and ice beads. In conclusion, the stereological method
365 provides a good quantification of the ice surface area and is consistent compared to µCT
366 measurements. The measurements could be improved by cutting thinner sections, which is, however,
367 technically difficult.
368 GBs are a very important property for snow chemistry and mechanical behaviour. Surprisingly, no
369 reference was found where the amount of grain boundaries was quantified and to what degree snow
370 was poly- or mono-crystalline. By combining stereology and polarisation microscopy, this could be
371 quantified for ice beads and for natural snow with some limitations.
372 The stereology method can also be used for natural snow samples; however, in this case of new snow,
373 which has very few and small grain boundaries, such a quantitative evaluation was not possible.
374 Image processing on µCT measurements (Theile and Schneebeli, 2011) allows, at least for rounded-
375 grain snow, for the estimation of the size and distribution of bonds without thin sections. However,

internal grain boundaries could not be detected. In the case of depth hoar, the geometry of the snow is too complex to discriminate GBAs with image processing. The problem, mainly in depth hoar, is that constrictions in the snow structure can be GBAs or simply a constriction in a mono-crystalline grain caused by the growth dynamic.

6. Conclusion

Design-based stereology provides consistent geometrical estimations of the samples. These results were confirmed by X-ray tomography. The SSA and the volume density calculated with both methods (stereology and μCT) were similar but show systematic differences. These differences are explained by the difficulty to define a unique surface of the ice grains for the stereological measurement. Furthermore, statistical analysis of the estimates confirmed that the stereological method and the sampling used are accurate. For snow types where a rotational isotropy in the vertical axis is justified, model-based stereology (as used in Matzl and Schneebeli, 2010) can be sufficient, and a simpler way of cutting is possible. The advantage of the design-based method presented here is that no assumptions are necessary. The additional effort in sample preparation is moderate. With the present stereological method, all snow types can be analysed, with the exception of new snow. The most important advantage of thin sections is the quantification of GBs because GBs cannot be observed with the μCT, and only for large grains using diffraction tomography (Rolland du Roscoat et al., 2011).

Acknowledgments

The authors thank M. Jaggi for the help in the preparation of the thin sections. The Swiss National Science Foundation supported the research, SNF grant 200020_125179. We thank S. Morin (CNRM-

400 GAME/CEN), L. Arnaud (LGGE) and an anonymous reviewer for the critical comments and
401 suggestions.
402

403 **REFERENCES**

404

405 Arakawa, H., Izumi, K., Kawashima, K. and Kawamura, T., 2009. Study on quantitative classification
406 of seasonal snow using specific surface area and intrinsic permeability. Cold Reg. Sci. Technol.,
407 59(2-3): 163-168. Doi: 10.1016/j.coldregions.2009.07.004.
408 Arnaud, L., Gay, M., Barnola, J.M. and Duval, P., 1998. Imaging of firn and bubbly ice in coaxial
409 reflected light: a new technique for the characterization of these porous media. Journal of
410 Glaciology, 44(147): 326-332.
411 Arnaud, L. et al., 2011. Measurement of vertical profiles of snow specific surface area with a 1 cm
412 resolution using infrared reflectance: instrument description and validation. J. Glaciol., 57(201):
413 17-29. Doi: 10.3189/002214311795306664.
414 Baddeley, A. and Vedel Jensen, E.B., 2005. Stereology for statisticians. Monographs on statistics and
415 applied probablility 103. Chapmann & Hall/CRC, 395 pp.
416 Baddeley, A.J., Gundersen, H.J. and Cruz-Orive, L.M., 1986. Estimation of surface area from vertical
417 sections. J Microsc, 142(Pt 3): 259-76. Doi: 10.1111/j.1365-2818.1986.tb04282.x.
418 Bader, H. et al., 1939. Der Schnee und seine Metamorphose. Erste Ergebnisse und Anwendung einer
419 systematischen Untersuchung der alpinen Winterschnee-decke, durchgefuhrt von der Station
420 Weissfluhjoch-Davos der Schweizerische Schnee- und Lawinenforschungskommis-sion 1934-
421 38. Beitr Geol Schweiz Geotech Ser Hydrol Lief, 3: 340p. + xxiii.
422 Brown, G.O., Hsieh, H.T. and Lucero, D.A., 2000. Evaluation of laboratory dolomite core sample size
423 using representative elementary volume concepts. Water Resour. Res., 36(5): 1199-1207.
424 Doi:10.1029/2000WR900017.

425 Cruz-Orive, L.M. and Weibel, E.R., 1981. Sampling designs for stereology. J Microsc, 122(Pt 3): 235-
426 57. Doi: 10.1111/j.1365-2818.1981.tb01265.x.
427 Davis, R.E. and Dozier, J., 1989. Stereological characterization of dry Alpine snow for microwave
428 remote sensing. Adv. Space Res., 9(1): 245-251.
429 Domine, F. et al., 2008. Snow physics as relevant to snow photochemistry. Atmos. Chem. Phys., 8(2):
430 171-208.
431 Fisher, D.S., Burns, J.C. and Pond, K.R., 1988. Estimation of mean and median particle size of
432 ruminant digesta. J Dairy Sci, 71(2): 518-24. Doi: 10.3168/jds.S0022-0302(88)79583-1.
433 Flin, F. et al., 2011. On the computations of specific surface area and specific grain contact area from
434 snow 3D images. Furukawa, Y., ed., Phys. Chem. Ice, Hokkaido University Press, Sapporo,
435 Japan: 321-328.
436 Good, W., 1987. Thin sections, serial cuts and 3-D analysis of snow. IAHS, 162: 35-48.
437 Gundersen, H.J., 1988. The nucleator. J Microsc, 151(Pt 1): 3-21. Doi: 10.1111/j.1365-
438 2818.1988.tb04609.x.
439 Gundersen, H.J. and Jensen, E.B., 1985. Stereological estimation of the volume-weighted mean volume
440 of arbitrary particles observed on random sections. J Microsc, 138(Pt 2): 127-42. Doi:
441 10.1111/j.1365-2818.1985.tb02607.x.
442 Gundersen, H.J., Jensen, E.B., Kieu, K. and Nielsen, J., 1999. The efficiency of systematic sampling in
443 stereology--reconsidered. J Microsc, 193(Pt 3): 199-211. Doi: 10.1046/j.1365-
444 2818.1999.00457.x.
445 Gundersen, H.J. and Osterby, R., 1981. Optimizing sampling efficiency of stereological studies in
446 biology: or 'do more less well!'. J Microsc, 121(Pt 1): 65-73.
447 Hildebrand, T. and Ruegsegger, P., 1997. A new method for the model-independent assessment of
448 thickness in three-dimensional images. J. Microsc. -Oxford, 185: 67-75. Doi: 10.1046/j.1365-
449 2818.1997.1340694.x.

Hobbs, P.V., 2010. Ice physics. Oxford University Press, Oxford, 837 S. pp.

Howard, C.V. and Reed, M.G., 1998. Unbiased stereology three-dimensional measurement in microscopy. Bios Scientific Publishers [etc.], Oxford, XVII, 246 pp.

Huthwelker, T., Ammann, M. and Peter, T., 2006. The Uptake of Acidic Gases on Ice. ChemInform, 37. 10.1002/chin.200625216.

Kaempfer, T.U., Schneebeli, M. and Sokratov, S.A., 2005. A microstructural approach to model heat transfer in snow. Geophysical Research Letters, 32(21): L21503. Doi: 10.1029/2005gl023873.

Kerbrat, M. et al., 2008. Measuring the specific surface area of snow with X-ray tomography and gas adsorption: comparison and implications for surface smoothness. Atmospheric Chemistry and Physics, 8(5): 1261-1275. Doi:10.5194/acp-8-1261-2008.

Kinosita, S. and Wakahama, G., 1959. Thin sections of deposited snow made by the use of aniline. Inst. Low Temp. Sci., 15: 35-45.

Lowe, H., Spiegel, J.K. and Schneebeli, M., 2011. Interfacial and structural relaxations of snow under isothermal conditions. J. Glaciol., 57(203): 499-510.

Mathieu, O., Cruz-Orive, L.M., Hoppeler, H. and Weibel, E.R., 1981. Measuring error and sampling variation in stereology: comparison of the efficiency of various methods for planar image analysis. J Microsc, 121(Pt 1): 75-88.

Matzl, M. and Schneebeli, M., 2010. Stereological measurement of the specific surface area of seasonal snow types: Comparison to other methods, and implications for mm-scale vertical profiling. Cold Regions Science and Technology, 64(1): 1-8. Doi: 10.1016/j.coldregions.2010.06.006.

Riche, F. and Schneebeli, M., 2011. Evolution of surface and grain boundary area in artificial ice beads used for experiments in snow chemistry. J. Glaciol., (submitted).

Rolland du Roscoat, S. et al., 2011. Analysis of snow microstructure by means of X-ray diffraction contrast tomography. Adv. Eng. Mater., 13(3): 128-135. Doi: 10.1002/adem.201000221.

Satyawali, P.K., Sinha, N.K. and Sethi, D.N., 2003. Double-microtoming technique for snow studies.

Can. J. Phys., 81(1-2): 529-537. Doi: 10.1139/P03-029.

Sterio, D.C., 1984. The unbiased estimation of number and sizes of arbitrary particles using the disector. J Microsc, 134(Pt 2): 127-36. Doi: 10.1111/j.1365-2818.1984.tb02501.x.

Theile, T. and Schneebeli, M., 2011. Algorithm to decompose three-dimensional complex structures at the necks: tested on snow structures. IET Image Proc., 5(2): 132-140. Doi: 10.1049/iet-ipr.2009.0410.

Tschanz, S.A., Burri, P.H. and Weibel, E.R., 2011. A simple tool for stereological assessment of digital images: the STEPanizer. J Microsc, 243(1): 47-59. Doi: 10.1111/j.1365-2818.2010.03481.x.

West, M.J., 1993. New stereological methods for counting neurons. Neurobiol Aging, 14(4): 275-85. Doi: 10.1016/0197-4580(93)90112-O.

FIGURE CAPTIONS

Fig. 1: *Micro-tomography of the ice beads. Some bonds between the grains are clearly visible but not the mostly polycrystalline structure of most beads.*

Fig. 2*: Sampling design for the ice beads using three randomly rotated vertical sections. The consecutive number indicates each step in the preparation. From a) to c), three sections perpendicular to the sample bottom/top are produced with systematically added angles, starting at a random angle. The blue "random 0-15" arrow means take a random number between 0 and 15 and place the cut this number of millimetres distant from the left tangent (a & c) and from the right b). The cuts (A - C) have to be strictly perpendicular to the bottom of the sample.*

Fig. 3: *Ice beads under polarised light microscopy. The upper grain is polycrystalline (yellow, blue and*

greyish colours), while the lower grain is monocrystalline. The blue circles mark an internal grain boundary area (IGBA), the red circle is a grain boundary area between two ice beads (GBA) and the green circle is the location of the surface are (SA), which corresponds to the interface between ice and air.

Fig 4: *Screenshot from STEPanizer, final version 1 (version 0.22). Yellow circles: intersections I between surface area and cycloids, Blue circles: points hitting the ice structure* P_{ice}.

Fig 5*: Thin sections of ice beads under crossed polarisers.*

Fig 6*: Relative error (%) between the stereological measurement and the X-ray measurement for the SSA and the volume density represented with box-plots. The stereological measurements give lower values than the* μCT-*measurements for the SSA and higher values for the volume density evaluations.*

Fig 7: *Vertical visualisation of a thin section. Only the surface of the thin section has to be taken into account in the stereological measurement.*

Fig 8: *Visualisation of the GBA segmentation using the image processing algorithm from (Theile and Schneebeli, 2011) of one of the ice bead samples.*

Fig 9*: Thin section of natural snow samples under polarised light. a) Small rounded grains, b) depth hoar.*

Table 1: *Comparison of the SSA and volume density between μCT and stereology for the ice beads. Also shown are the values for the specific grain boundary areas (SGBA, SIGBA). The statistics of the relative errors are plotted in Fig. 6.*

Table 2: *Comparison of the SGBA (mm-1) evaluated using the image-processing algorithm by Theile and Schneebeli (2011) and stereology for eight samples of ice beads. Ice beads are very well segmented using the image-processing algorithm (see also Fig. 8).*

Table 3: *Relative error between μCT measurements and stereology measurements for 3 types of snow: small rounded grains (see also Fig 7a), depth hoar (see also Fig 7b), depth hoar 2 (with a higher density than "depth hoar").*

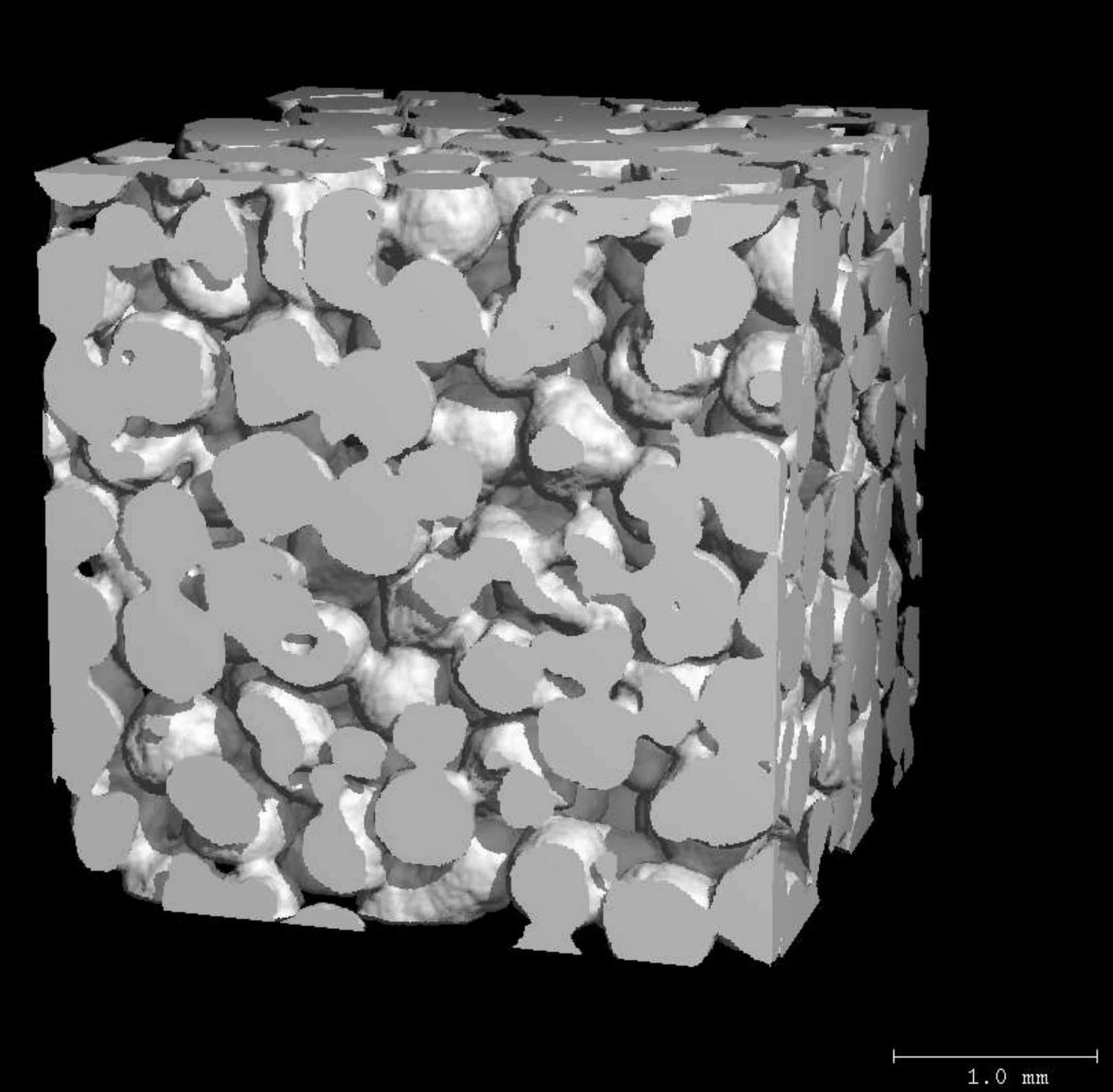
1.0 mm

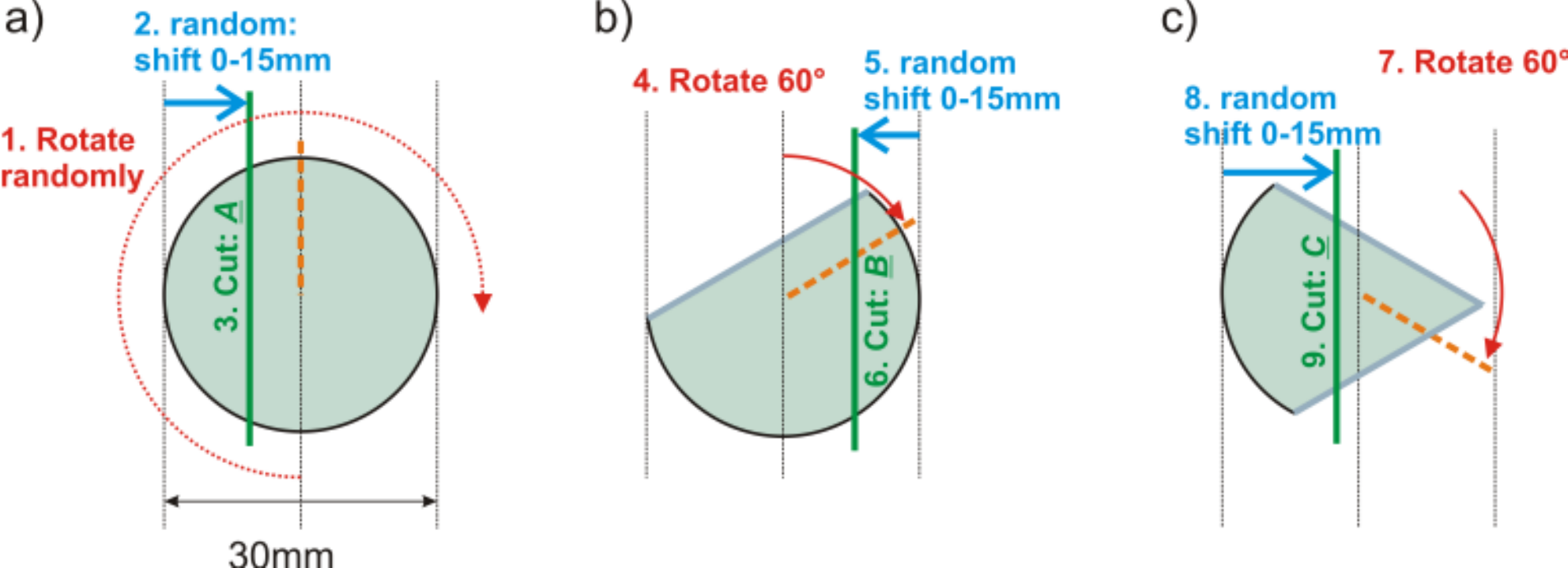
a)
2. random:
shift 0-15mm
1. Rotate
randomly
3. Cut: A
30mm
b)
4. Rotate 60°
5. random
shift 0-15mm
6. Cut: B
c)
7. Rotate 60°
8. random
shift 0-15mm
9. Cut: C

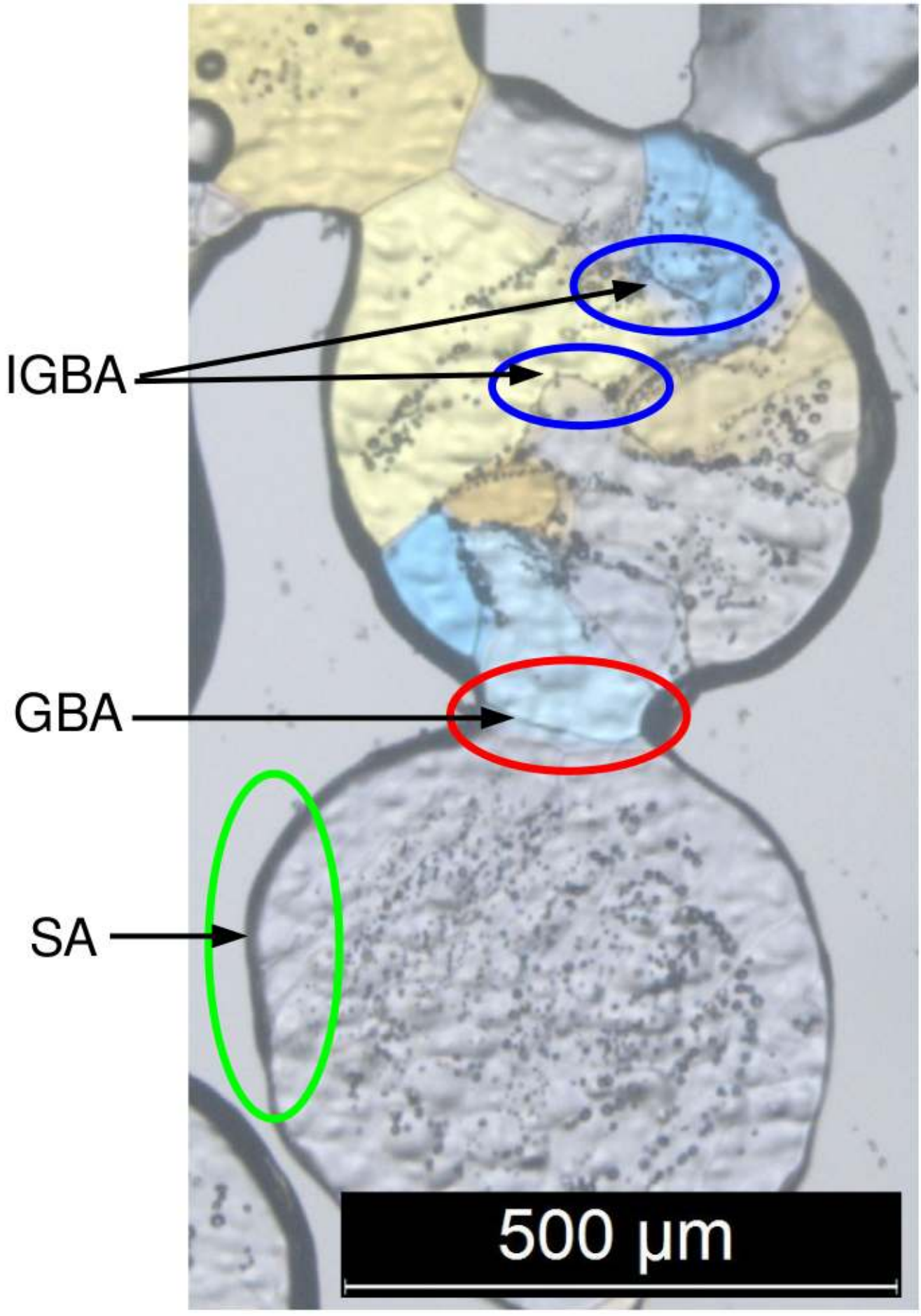
IGBA
GBA
SA
500 µm

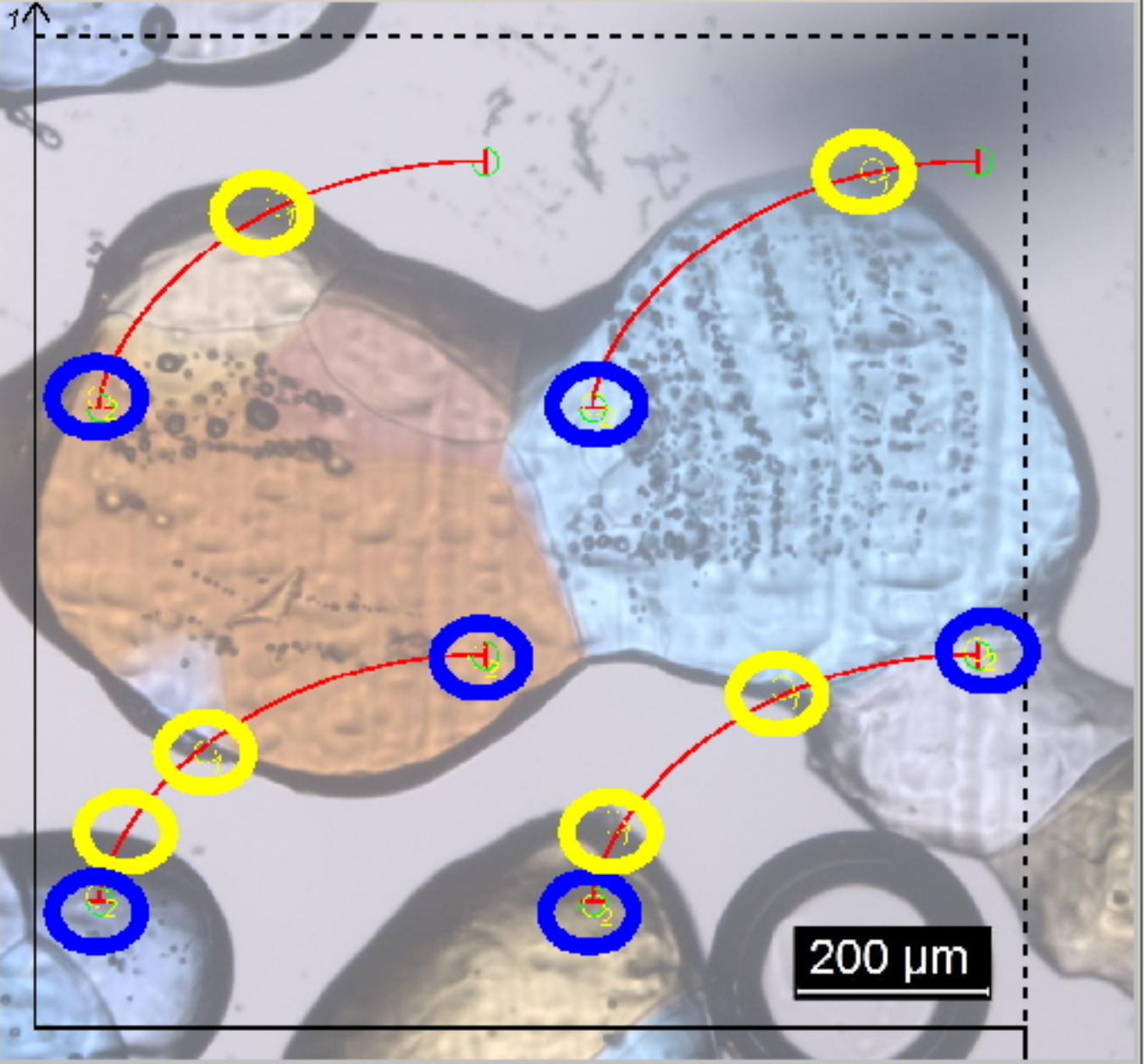
200 µm

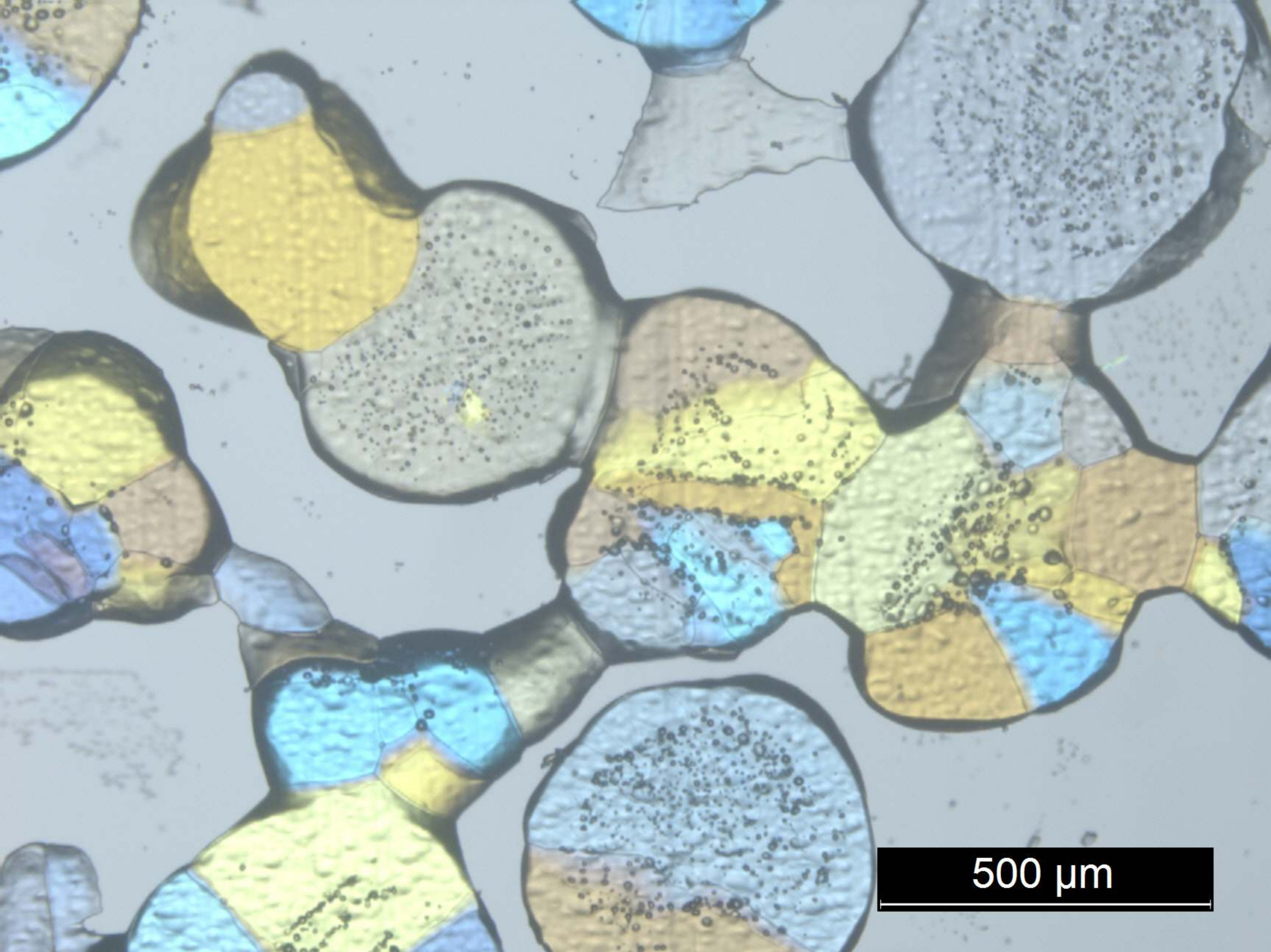
500 µm

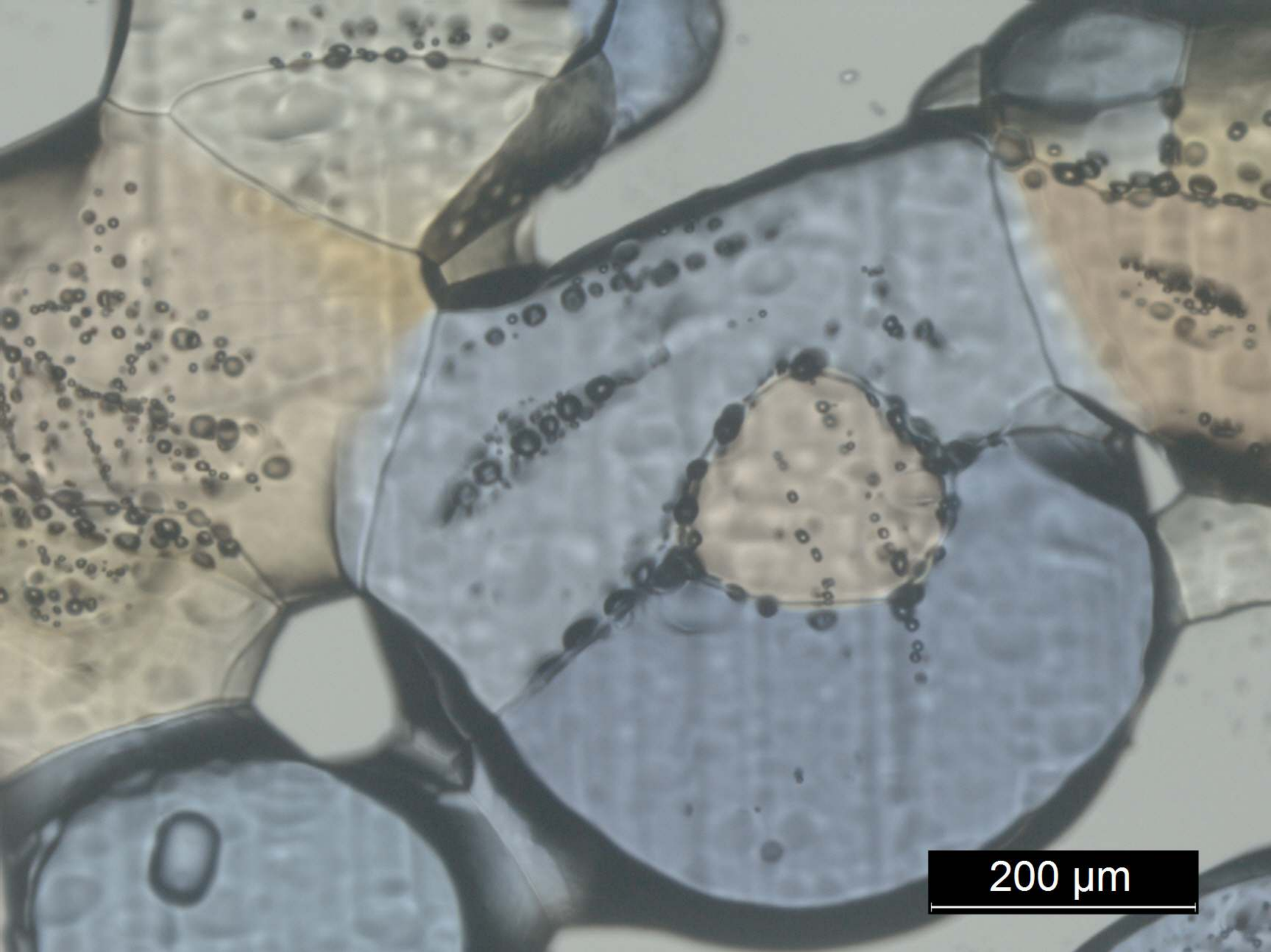
200 µm

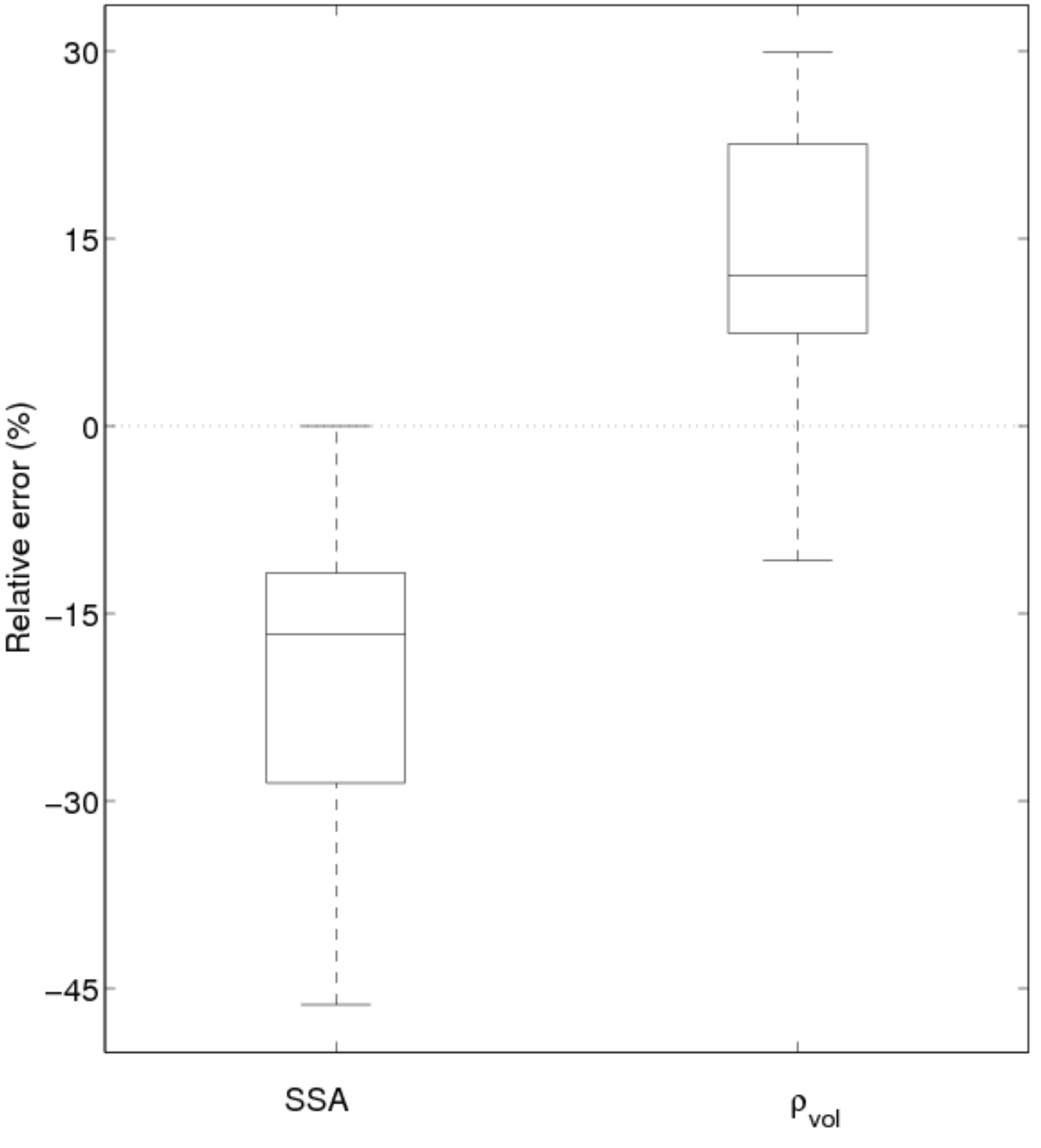
30
15
0
−15
−30
−45
Relative error (%)
SSA
ρ_{vol}

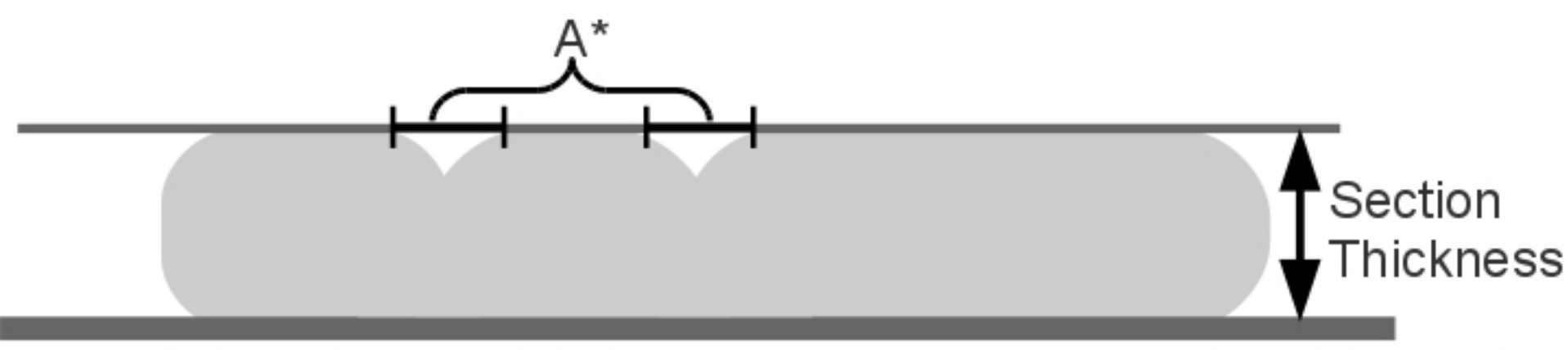

A*: These two areas do not belong to the surface of the section, which have to be taken into account in the stereology measurement.

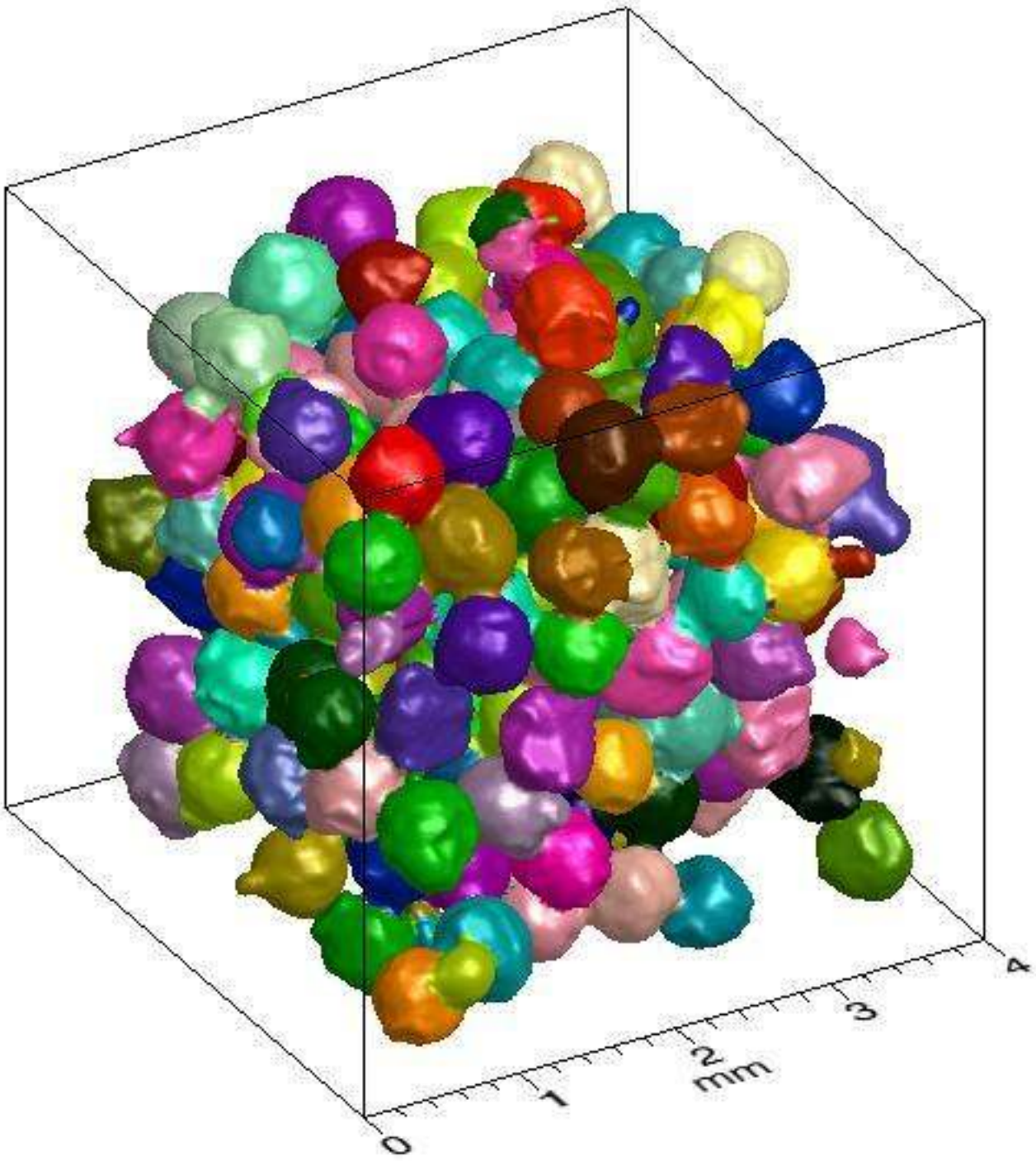
0
1
2
3
4
mm

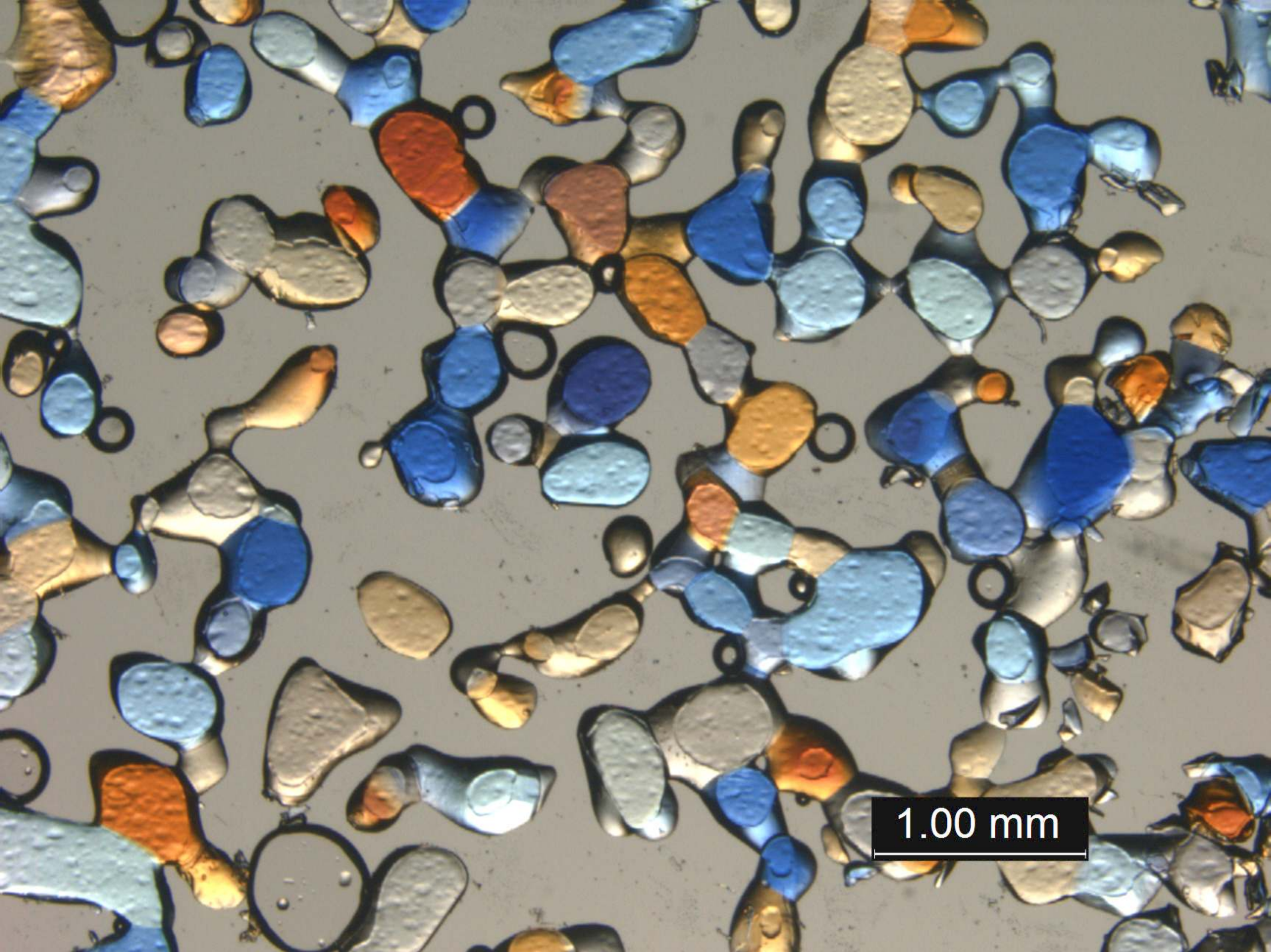
1.00 mm

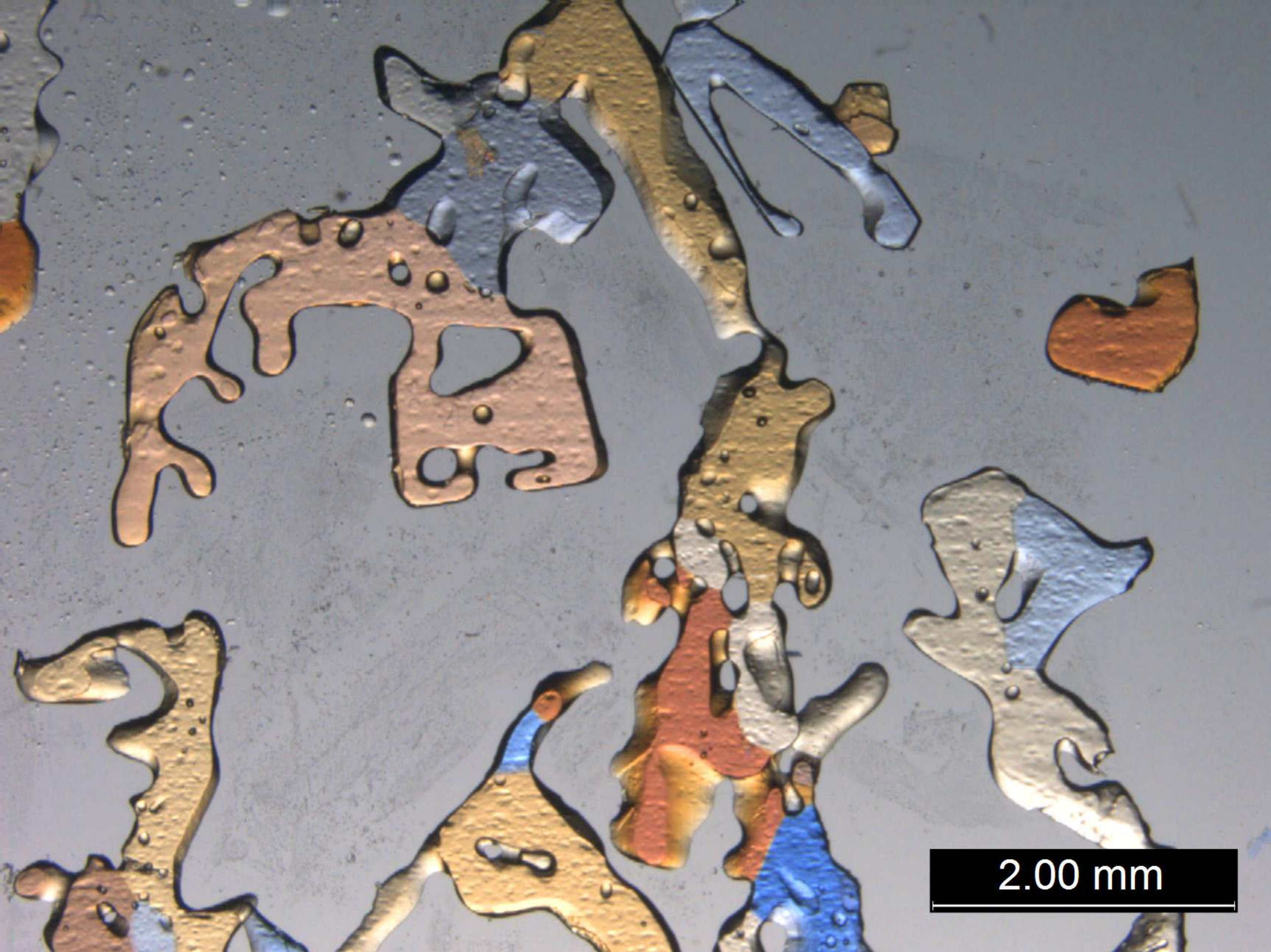
2.00 mm

Table 1: Comparison of SSA and volume density between µCT and stereology for the ice beads. Also shown are the values for the specific grain boundary areas (SGBA, SIGBA). The statistics of the relative errors are plotted in Fig. 6.

Sample	µCT		Stereology				Relative error (%)	
	SSA (mm^{-1})	ρ_{vol} (%)	SSA (mm^{-1})	ρ_{vol} (%)	SGBA (mm^{-1})	SIGBA (mm^{-1})	SSA	ρ_{vol}
1	11.48	49.9	7.51	62.0	1.27	7.67	*-34.56*	*24.21*
2	10.76	50.4	9.72	58.3	1.26	8.17	*-9.59*	*15.83*
3	9.70	51.6	7.38	67.0	1.51	5.02	*-23.97*	*29.88*
4	12.06	58.3	7.21	74.0	1.30	7.46	*-40.22*	*26.77*
5	11.51	59.3	7.87	70.9	0.85	8.35	*-31.65*	*19.69*
6	10.56	58.0	5.67	71.4	0.82	/	*-46.31*	*23.20*
7	10.14	54.9	8.95	60.2	1.90	8.40	*-11.73*	*9.57*
8	10.40	56.9	10.40	64.4	1.49	6.68	*0.01*	*13.28*
9	10.41	55.6	8.82	54.0	1.78	5.98	*-15.34*	*-3.00*
10	10.06	59.5	8.44	63.9	1.62	5.85	*-16.04*	*7.43*
11	9.84	57.3	7.03	53.2	1.59	4.53	*-28.57*	*-7.25*
12	8.73	58.8	7.40	64.2	1.42	4.98	*-15.30*	*9.13*
13	9.15	60.2	7.35	53.7	0.98	5.44	*-19.68*	*-10.79*
14	8.51	59.8	7.55	56.3	1.46	4.80	*-11.31*	*-5.89*
15	9.71	57.7	8.21	64.0	1.44	4.61	*-15.45*	*10.90*
16	8.75	55.0	7.11	67.4	1.38	4.11	*-18.78*	*22.56*
17	9.28	57.7	7.68	62.5	1.35	4.67	*-17.25*	*8.39*
18	8.51	52.7	8.34	62.0	1.59	3.81	*-1.91*	*17.74*

Table 2: Comparison of SGBA (mm^{-1}) evaluated using the image-processing algorithm by Theile and Schneebeli (2011) and stereology for eight samples of ice beads. Ice beads are very well segmented using the image-processing algorithm (see also Fig. 8).

Sample	SGBA min (mm^{-1})	SGBA max (mm^{-1})	SGBA stereo (mm^{-1})
Ice beads	0.89	1.41	0.82
Ice beads	1.13	1.70	1.49
Ice beads	1.09	1.71	1.62
Ice beads	1.13	1.71	1.78
Ice beads	1.24	1.88	1.59
Ice beads	1.23	2.02	1.44
Ice beads	1.33	2.15	1.35
Ice beads	1.62	2.46	1.59
Small rounded snow	1.83	2.76	2.91

Table 3: Relative error between µCT measurements and stereology measurements for 3 types of snow: small rounded grains (see also Fig 9a), depth hoar 1 (see also Fig 9b), depth hoar 2 (with a higher density than "depth hoar 1").

Snow type	µCT		Stereology			Relative error (%)	
	SSA (mm^{-1})	ρ_{vol} (%)	SSA (mm^{-1})	ρ_{vol} (%)	SGBA (mm^{-1})	SSA	ρ_{vol}
Small rounded	11.22	35.4	12.01	29.1	1.71	7.04	-17.80
Depth hoar 1	6.56	27.1	7.75	21.0	1.91	18.14	-22.51
Depth hoar 2	9.35	41.0	8.21	51.6	1.81	-12.19	25.85